



Electron beam welding of copper using plasma spraying for filler metal deposition

M. Stummer¹ · M. Stütz¹ · A. Aumayr¹ · N. Enzinger¹

Received: 30 May 2018 / Accepted: 3 August 2018 / Published online: 29 August 2018
© The Author(s) 2018

Abstract

Due to physical properties like high thermal and electrical conductivity, joining of copper is of special interest in steelmaking or electrical industry. Unfortunately, joining of thick-walled copper components using electron beam welding (EBW) tends to welding defects like insufficient root formation or varying penetration depth. In previous investigations, Cu-DHP (deoxidised high phosphorus copper) plates were successfully joined by EBW utilising a CuSn6 sheet as filler material. The investigation resulted in a stable EBW parameter window. Nevertheless, using CuSn6 sheets lead to challenges concerning joint preparations, and is not usable for arbitrary weld configurations. To meet these challenges, atmospheric plasma spraying (APS) is used to apply a thin interlayer in the welding zone and substitute the CuSn6 sheet filler metal. This continuative work includes further improvements of the main EBW parameters and uses APS as a new approach for filler metal deposition. Furthermore, determining and enhancing the service properties of the copper joints is of main interest and reported here.

Keywords Copper · EBW · Atmospheric · Plasma spraying · APS · Welding of large cross sections · Filler metal deposition by APS

1 Introduction

Arc welding of copper and its alloys is challenging due to its high thermal conductivity and resulting welding defects, like root suck back or hot cracking [1, 2]. To prevent these welding defects, different requirements in regard to the welding process have to be fulfilled. One requirement is the use of a highly concentrated heat input. Electron beam welding (EBW) is a suitable technology, which meets this requirement. However, the concentrated heat input of EBW results in narrow heat affected zones, high temperature gradients and fast cooling rates, which are influencing the behaviour of the weld pool and encourage welding defects, like periodically occurring cracks, spiking, or inconsistent penetration depths [1, 3]. These welding defects can be prevented only by correct process handling.

In a previous investigation, a systematic parameter study led to a stable welding process and successful copper joints were generated. By inserting a CuSn6 sheet as filler material, the behaviour of the weld pool could be successfully stabilised. A linear decreased energy input per length unit during welding was chosen to overcome preheating effects due to the material's high thermal conductivity. The combination of the parameters and using a filler material led to a stable root formation and a significant reduction of spiking defects [4].

However, using sheets as filler material leads to new challenges related to joint preparation of arbitrary geometries, where an insertion of sheets may be complicated or even impossible. To address these new challenges, the used CuSn6 sheets are substituted with thin Sn interlayers deposited by atmospheric plasma spraying (APS) as filler metal [5, 6].

This continuative work gives an insight to an alternative filler material deposition method, further improvements of the applied EBW parameter set and the characterisation of the joints regarding their service properties.

Recommended for publication by Study Group RES - Welding Research Strategy and Collaboration

✉ M. Stummer
maximilian.stummer@tugraz.at

2 Materials and methods

The experiments were divided in three independent steps. First, the filler metal was deposited locally on the base metal

¹ Institute of Materials Science, Joining and Forming, Graz University of Technology, Kopernikusgasse 24, 8010 Graz, Austria

Table 1 Nominal chemical composition of Cu-DHP in wt%

	Copper	Phosphorus
	99.9	0.015–0.04

by APS. This alternative approach manifests in high flexibility and stability and suits also with complex component geometries. In detail, three different layer thicknesses were investigated systematically. Second, the APS-coated copper plates were subsequently welded by the electron beam technique. Finally, an extensive investigation of the functional properties of the final joints was conducted. Hence, physical and mechanical properties are in the focus.

2.1 Base metal

Copper and copper alloys are well-known for their physical properties like high thermal and electric conductivity. Therefore, typical applications of copper components are chill moulds, heat exchangers and electric conducting paths. Especially electric conducting paths, which are related to high current densities and large cross-sections, are often clamped or fastened using screws or bolts, which tends to high costs of material preparation like machining to high surface quality as well as a significant local loss of its properties.

The copper alloy which is used in this study is Cu-DHP, which is de-oxidised copper with limited remnant content of phosphorus. Due to its phosphorus content, the material shows enhanced weldability, brazeability and resistance to hydrogen embrittlement. Table 1 shows the nominal chemical composition of the Cu-DHP base material.

The dimensions of the investigated copper plates are 100 × 50 mm with a thickness of 30 mm. Although, beam welding of thin copper sheets can be handled quite easily,

material thicknesses of more than 30 mm tend to characteristic welding defects like spiking and root ‘suck back’. These challenges cannot be sufficiently handled by adjusting the welding parameters or special weld seam preparation [4].

2.2 Filler metal

The root cause of the before mentioned problems is found on the melting and solidification behaviour of copper alloys as well as in the thermo- and fluid-dynamic properties of the copper melt. Introducing specific alloying elements lead to a change of the melt pool behaviour and the physical properties of the final joint [7]. Especially by adding small amounts of Sn the viscosity of the liquid changes significantly, which has some potential to improve the weld seam formation and geometry, Sn bronzes are classified as Cu-Sn alloys with a Sn content up to 12% [8]. If the Sn content exceeds that amount, detrimental and partly brittle η -, ϵ - or ζ - phases occur, which impair the technological applicability of the joint. Figure 1 shows the development of surface tension and viscosity fraction of the Cu-Sn system [10]. Three factors could be distilled for improving the melt pool behaviour. First, an alloy exhibits a melting interval rather than a melting temperature, which is crucial for developing a stable weld pool during welding. Second, a slight non-linear decrease of surface tension (Fig. 1) can be observed at a mole fraction of 0.1. Third, by adding 12% Sn to Cu, the behaviour of viscosity changes slightly in a certain temperature interval [10], which can lead to an improved material flow. Hence, it is assumed that local alloying has a positive effect on root formation. Due to the overall low Sn content, no brittle intermetallic compounds should be formed [11].

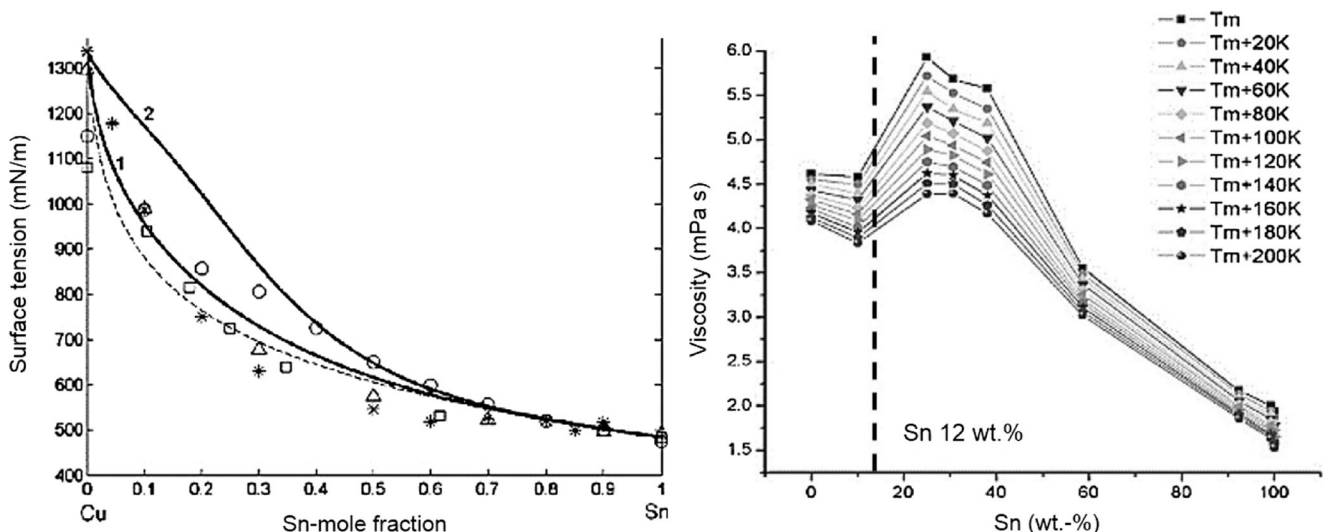


Fig. 1 Surface tension [9] and viscosity of molten Cu-Sn alloys in correlation of temperature and Sn content [10]

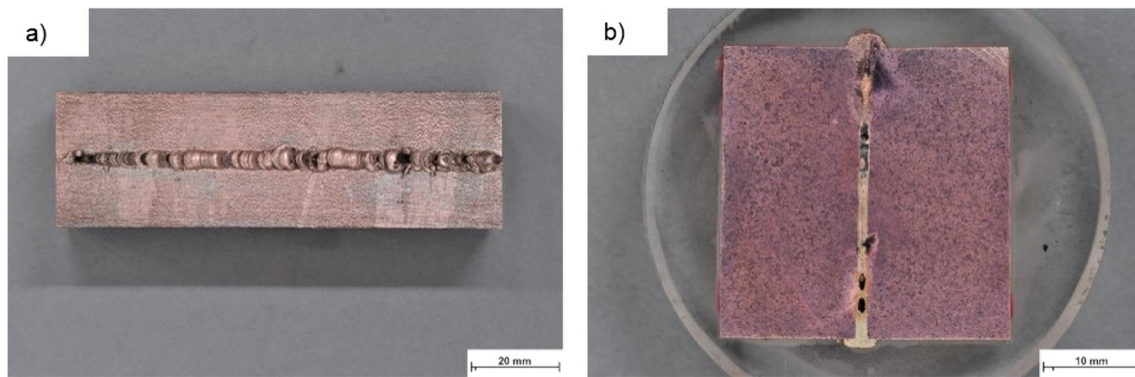


Fig. 2 EB welds of 30-mm thick copper plates with characteristic defects due to Sn paste filler application **a** irregular weld bead formation, sinkholes **b** strong void formation and porosity in the welding zone [11]

Consequently, although one major benefit of EBW is a filler metal free process, using filler metal enables a possible control of the welding process stability as well as the melt behaviour during solidification.

In a first step, the feasibility of this approach was proven by using CuSn6 sheets as a filler material between two blocks to be welded. However, for complex geometries, bulk filler metals like CuSn6 sheets are not a reasonable method. An adaptive and stable filler metal application process is required. Therefore, different processes were investigated previously:

- Manually adding Sn paste
- Atmospheric plasma spraying

It became evident that a homogeneous interlayer is required, which was not sufficiently the case by manually adding a Sn paste. Figure 2 gives an overview of the resulting welds using a Sn paste as interlayer. Using Sn paste led to high porosity within the whole specimen, especially in the top and root zone of the weld.

A metallographic investigation indicated that APS is a much more promising approach to add filler material locally in the welding zone. This approach will be presented in the following sections.

2.3 Atmospheric plasma spraying

APS is designated as a thermal spray process and is often used to deposit functional layers, like corrosion, biomedical or wear resistant layers [12, 13]. Applying filler metal by APS is a promising approach and brings two major advantages. First, complex geometries can be coated easily, whereby no vacuum or shielding gas is required. Second, the automatic APS process is stable, reproducible and can be applied locally on various substrate materials. Consequently, the process is also suitable for different filler materials, including metallic, ceramic and complex powder compositions. This leads to numerous possible material combinations.

By using spherical shaped pure Sn particles with an average diameter of 25 μm very thin and homogenous layers can be produced. The used particle size and distribution are indicated in Fig. 3.

In order to enhance the wetting behaviour of the copper substrate, the surface undergo a thermal activation and cleaning process. This thermal process leads to vaporisation of small particles and residues, as well as an increase of the surface energy, which directly influences the adhesive strength of the layer. This phenomenon can be observed in various material combinations [14–17]. After the activation step, the

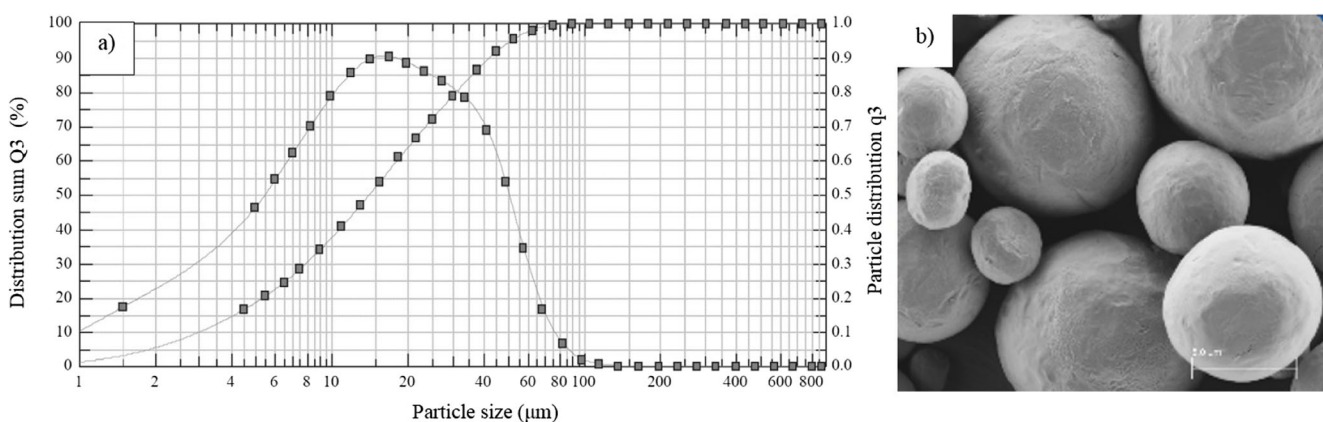


Fig. 3 **a** Size and distribution of the used Sn particles (VP68036/G); **b** spherical Sn particles used for APS

Table 2 Main activation and APS parameters [17]

	Electric current (A)	Feed speed (mm/s)	Working distance (mm)	Powder type (/)
Activating	150	100	20	–
Coating	45	300	21	VP68036/G [15]

subsequent APS process starts. The Sn particles are molten in a plasma arc and accelerated by process gas (argon, 5 bar) towards the substrate material. Table 2 shows the main activation and plasma spraying parameters. These parameters are the electric current (I), the feed speed (v) and the working distance (a), as well as the used powder material. The plasma gas flow rate is set constant with 10 l/min, and the powder feed rate is set to 5 g/min. Pure argon is used as process gas.

Figure 4 shows the APS-coated copper part and one representative cross-section of the Sn interlayer. After the process, the final interlayer thicknesses of 15, 30 and 45 μm were achieved.

The interlayer thicknesses were previously volumetrically calculated to ensure a similar nominal composition of the previously investigated CuSn6 sheet filler metal to ensure comparable welds seam properties [4]. The porosity of the interlayer was determined on representative cross-sections with 15%.

2.4 Electron beam welding

EBW enables single pass welds of large cross-sections of, e.g., high-strength steel sheets with thicknesses of more than 100 mm, due to a highly focused high energy beam ($> 10^5 \text{ W/mm}^2$). Furthermore, the high energy densities allow very small and narrow heat-affected zones, reduce local hardness peaks and enhance the service properties of the produced welds in general [18]. EBW is generally conducted in high vacuum ($< 10^{-3}$ mbar) and therefore no oxidation occurs. Thick-walled copper components tend to an increased heat sink and require a preheating step to ensure a proper joint, which results in high costs. By using EBW the preheating step is not necessary, due to a very local heat input, which is a

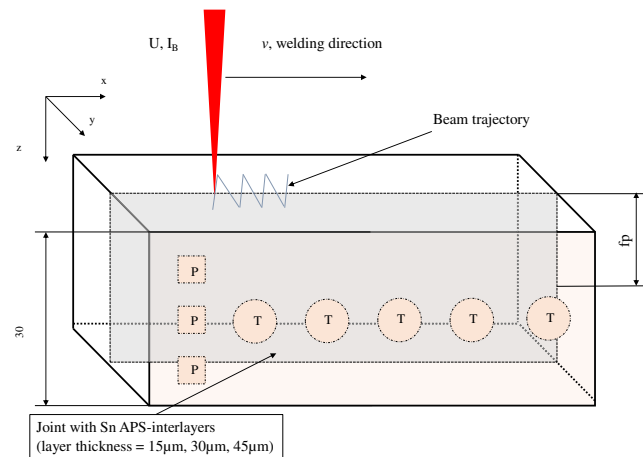


Fig. 5 Schematic of the welding experiments; red-shaded areas indicate the positions of transverse tensile specimen (T) and potentiostatic test specimen (P)

major advantage [1]. Figure 5 shows a schematic sketch of the joint and the main EBW parameters. The investigated EBW parameters are as follows:

- Acceleration voltage— U (kV)
- Primary beam current— I_B (mA)
- Welding feed speed— v (mm/s)
- Focus point— fp (mm)
- Beam deflection figure (triangle) with y -amplitude dy (mm)
- Deflection figure frequency— f (Hz)

The limited heat dissipation of the copper parts leads to an unavoidable temperature increase of the base material during welding. This preheating further leads to an increase in penetration depth over welding distance. To countervail this effect, the energy input per length unit was reduced by linearly increasing the welding speed from 5 to 9 mm/s during welding. This leads to a linear decrease of the line energy input and a welding time of 14 s per pass [4]. Furthermore, to improve dilution and degassing during welding, two welding passes were performed. In a preliminary investigation, different

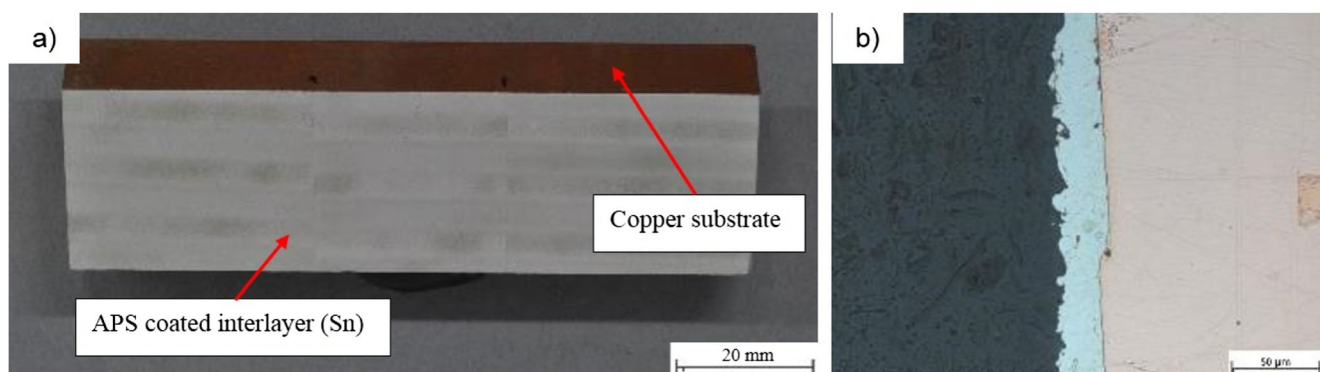


Fig. 4 APS-coated copper substrate **a** tin interlayer as filler metal **b** cross-section of the Sn interlayer

Table 3 EBW parameter set

	U (kV)	I_B (mA)	v (mms ⁻¹)	Fp (mm)	figure	Dy (mm)	f (Hz)
Welding pass 1	150	100	5–9	–15	Triangle	1	1000
Welding pass 2	150	140	5–9	–15	Triangle	1.5	30

parameter sets were tested. It became evident that changing the frequency and geometry of the beam figure led to better dilution of the weld zone. Both welding passes were designed for full penetration. In detail, the y-amplitude of the beam figure of welding pass 2 was increased from 1 to 1.5 mm; hence, the beam power was increased accordingly. The final parameter set is displayed in Table 3.

2.5 Tensile tests

Quasi static cross tensile tests were performed for all welds using cylindrical tensile specimens ($\varnothing 8 \times 100$ mm) to characterise the tensile strength. A crosshead speed of 3 mm/min was used for all experiments.

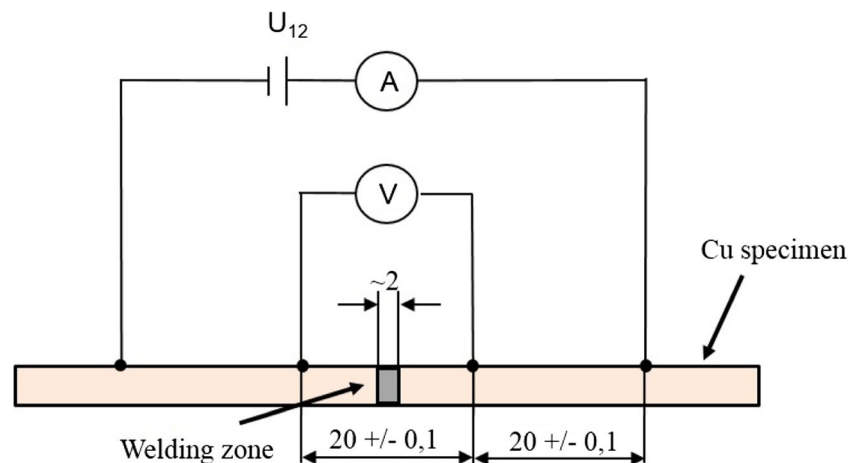
2.6 Potentiostatic investigation

Measuring the electrical resistivity of copper in general requires measuring technique with a high sensitivity. To fulfil this requirement, four-point potentiostatic measurement with a resolution of $1 \mu\Omega$ was chosen.

Figure 6 shows a sketch of the measuring setup and the investigated welding zone. Based on the measured data, an electrical resistance R_{measured} was recorded and the specific electrical conductivity λ was calculated (Eqs. 1 and 2). Thus, A represents the specimen cross-section and L represents the measuring length (20 ± 0.1 mm).

$$\rho = \frac{R_{\text{measured}} * A}{10^6 * L} * \left(\frac{\Omega \text{mm}^2}{\text{m}} \right) \quad (1)$$

Fig. 6 Schematic of the measurement setup. A four-point potentiostatic measurement with in a total measuring length of 60 mm. The welding zone was defined as 2 mm



$$\lambda = \frac{1}{\rho} * \left(\frac{\text{m}}{\Omega \text{mm}^2} \right) \quad (2)$$

However, since the electric conductivity of the welding zone is of major interest, base and weld metal has to be distinguished. Therefore, the size of the fusion zone was measured by light optical microscopy (LOM). According to the LOM investigation a welding zone width of about 2 mm could be defined for all investigated specimen. Based on that analysis, the base material was deduced by Ohm's law of all investigated samples and the specific electric resistivity of 2 mm welding zone could be determined as a function of the different interlayer thicknesses.

Since a measurement with the present resolution is very easily distorted by ambient influences, all measurements had to be performed at defined room temperature (20 °C) and humidity (40%) to ensure identical measurement conditions.

2.7 Computer tomographic investigation

The CT-scans were performed by an industrial RayScan 250E CT-device, equipped with a 225 kV μ -focus X-ray tube and a 2048×2048 pixels flat panel detector. A set of 2D projection images is acquired during a full rotation of the specimen, which is finally used to reconstruct a 3D image of the specimen consisting of volumetric pixels (voxels) by typically using a filtered back-projection algorithm [19]. Voxels are represented as grey values, which mainly correspond to the density and atomic number of the penetrated material at the particular position within the specimen. Micro-focus tubes are defocusing the electron beam proportionally to the electric

Table 4 CT parameters

	<i>U</i> (kV)	<i>I</i> (μ A)	Pre-filter copper	Integration time (s)	Scanning time (min)	Voxel size (μm^3)
RayScan 250E	150	50	0.5	3	115	1000

power, to prevent the tungsten target from thermal destruction. The electric power has been set in accordance with the voxel size, to ensure a minimum image blurring caused by the focal spot of the X-ray tube. The CT-scans have been performed with a voxel size of about $6 \mu\text{m}^3$. The main CT parameters are shown in Table 4.

3 Results and discussion

3.1 Weld bead formation

A regular weld bead was formed with a homogeneous chevron pattern on the top surface and a regularly formed root appearance. Spattering during welding was low and no large inhomogeneities were observed with all three Sn layer thicknesses. The light optical microscopy (LOM) showed the characteristic weld bead collapse on the top side of the joint. This collapse is based on gravity directed material flow during EBW and re-solidification. Introducing a thicker Sn interlayer into the welding zone leads to an increased liquid metal flow in root direction, due to a decrease in viscosity. Consequently, the volumetric weld bead decline gets more significant and leads to a more pronounced root formation. Figure 7 shows the top position and the root of the EB welds according to different interlayer thickness. The LOM investigation reveals also an increased amount of tin residues in the root area at $45 \mu\text{m}$ interlayer thickness.

The primary pore formation takes place in the root area of the joint, due to material flow. However, the achieved porosity using Sn plasma interlayers is superior, compared to copper joints using Sn paste as filler metal. In addition, the process is more stable and the weld bead is regular. Table 5 gives an overview about the weld bead characteristics and geometries. The differences of weld bead decline and the resulting excessive root material are due to the unevenly distributed root evolution in welding direction.

Figure 8 shows representative cross-sections of the investigated welds. Due to the overall low Sn content in the weld, no brittle intermetallic compounds were found by SEM investigation. However, the LOM investigation of the welding samples led to the assumption that the influence of the microstructure has a minor impact on the mechanical properties of the welds.

3.2 EDX investigation of the remaining Sn content

To determine the Sn content in the welding zone, an energy dispersive X-ray (EDX) analysis transversely to the joint was performed. No Sn could be detected in the top or middle zone of the weld. It becomes evident that Sn accumulates in the root area, majorly in the peripheral zone of the excessive root material. Additionally, Sn residues could only be detected the root area (Fig. 9). This behaviour is related to the 1.4 times higher density of Cu compared to pure Sn.

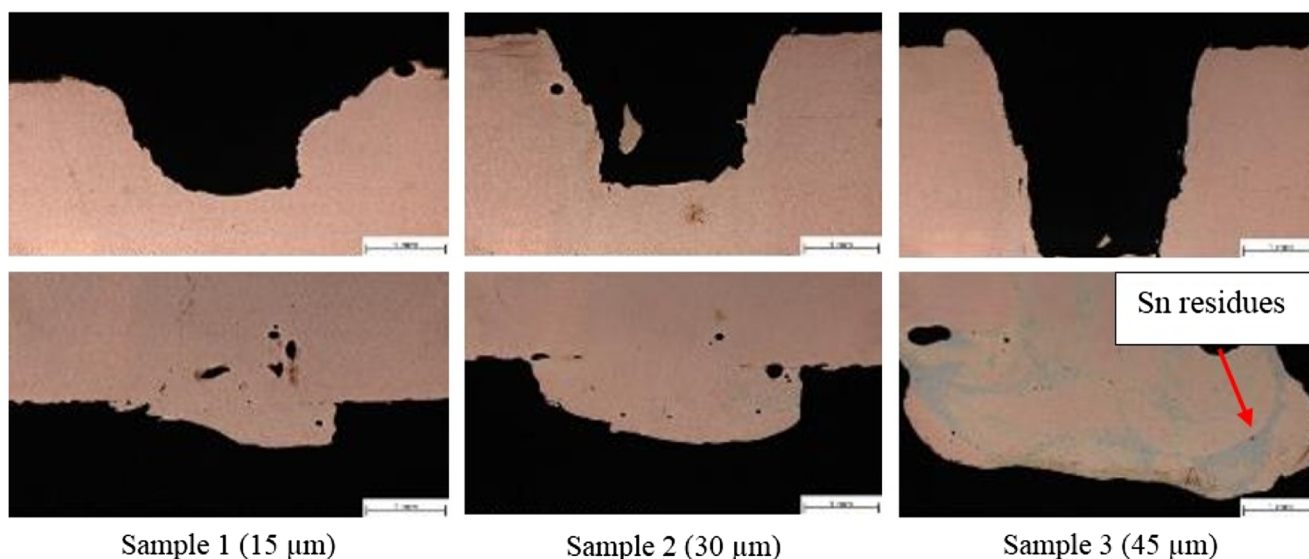


Fig. 7 Top and bottom (root) position of the welds depending of the interlayer thickness (not etched)

Table 5 Evaluation of the weld bead geometry using APS interlayers

Sample	Layer thickness (μm)	Weld bead decline (mm^2)	Excessive root material (mm^2)	Porosity (%)
S1	15	3.896	1.174	1.3
S2	30	4.638	3.638	0.9
S3	45	7.074	9.133	1.2

This leads to the assumption that the thin Sn layer destabilises the weld pool and changes the viscos-physical properties of the molten material, rather than generating a Cu-Sn solid solution in the joint. The destabilisation increases with the Sn content, which can be observed in a more pronounced root formation.

3.3 Tensile strength

The results show a tensile strength of about 90% of the base material (Fig. 10). Alloying the welding zone with different tin interlayer thickness, lead to a small variation of tensile strength. However, the results are also comparable with bead-on-plate welds. Therefore, Sn is not the only reason to reduce the strength; it is mainly caused by the welding process itself. Due to different material properties in the welding zone and the base material, the elongation before fracture and yield stress was not taken into account for further investigation.

3.4 Electric conductivity

Overall, the electron beam welds show a substantial improvement compared to clamped condition, which is state-of-the-art in electric engineering [20]. Figure 11 shows no major differences through all investigated EBW samples (S1, S2, S3). However, there is a slight decrease of electric conductivity compared to base material. The lowest values were measured with an interlayer thickness of 30 μm , 45 and 15 μm exhibit values closer to the bead-on-plate weld.

3.5 Porosity

Since the measurement results could not show a clear relation between interlayer thickness and electrical conductivity, a computer tomographic (CT) investigation was performed to evaluate the porosity of the copper joints in the bottom (root) zone of the EBW joints. Figure 12 shows the result of the CT investigation of the EBW samples and the bead-on-plate weld at bottom (root position).

This investigation shows that local alloying significantly improves the quality of the joint with respect to porosity. However, this improvement is not recognisable in strength or conductivity. The CT investigation of the bead-on-plate welds show signs of spiking and high porosity, due to the absence of Sn. According the preliminary investigation [4] and literature [21], the instable keyhole behaviour can be a possible cause of this spiking phenomenon.

Although the bead-on-plate welds show very high pore density within the welding zone, the specific electric conductivity is comparable to the other specimens. This suggests that the electric conductivity is not strongly coupled to porosity within the tested Cu-DHP material, but is more affected by the tin content—even in very small amounts.

4 Summary and conclusion

EBW of thick-walled copper components (> 30 mm) tends to different welding defects like spiking, insufficient root formation or porosity. These defects cannot be simply handled by

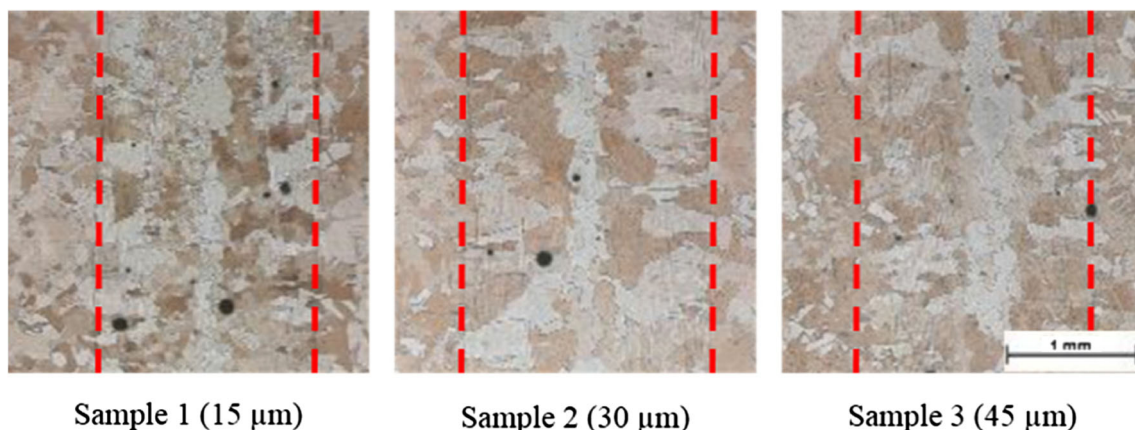


Fig. 8 Representative cross-sections of the investigated Cu welds. The red-dashed line indicates the welding zone

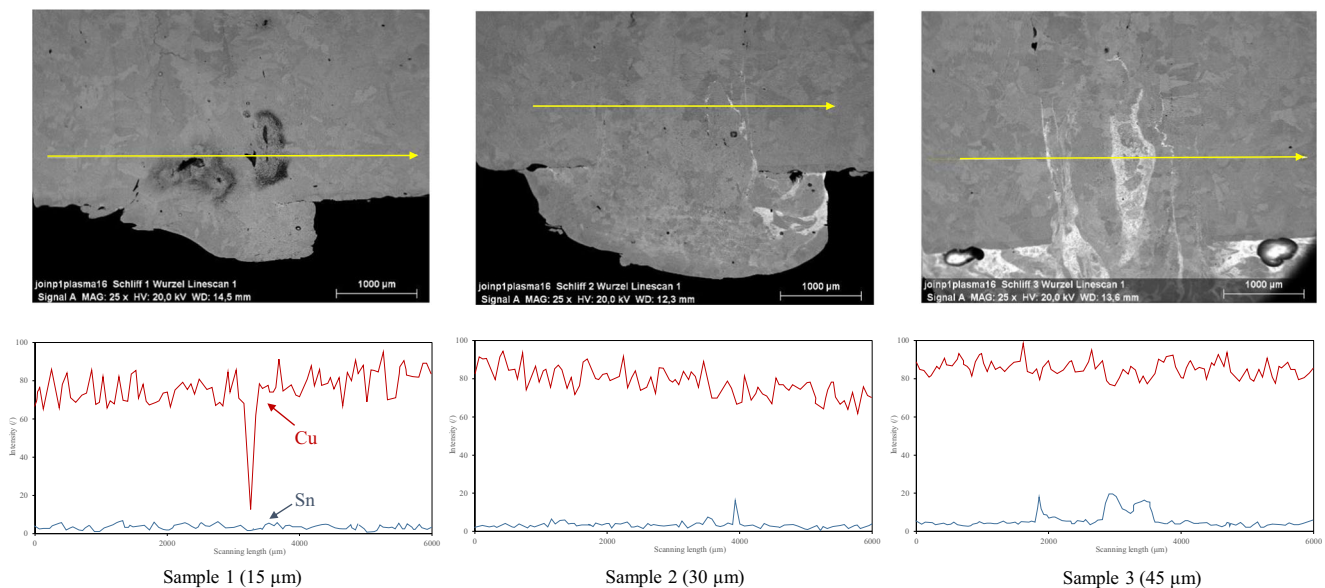


Fig. 9 EDX line scan of the root depending on the interlayer thickness. Bright areas show higher tin content—see bottom line of histogram

Fig. 10 Measurement of the tensile strength of welds with different interlayer thickness and bead-on-plate. The dashed line indicates the tensile strength of the base material (Cu-DHP)

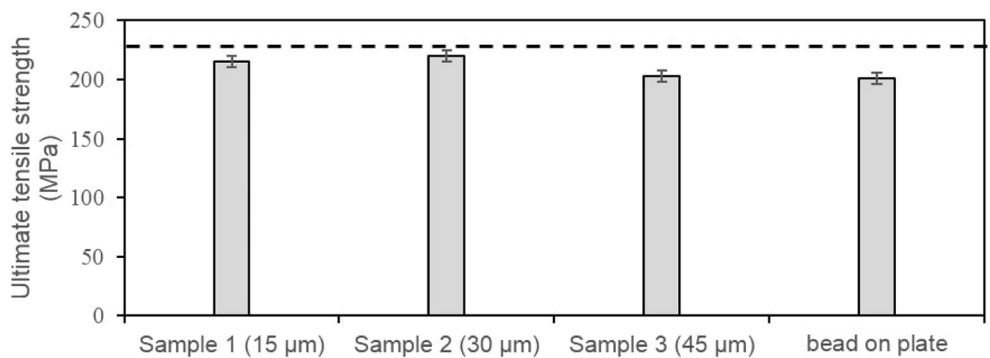
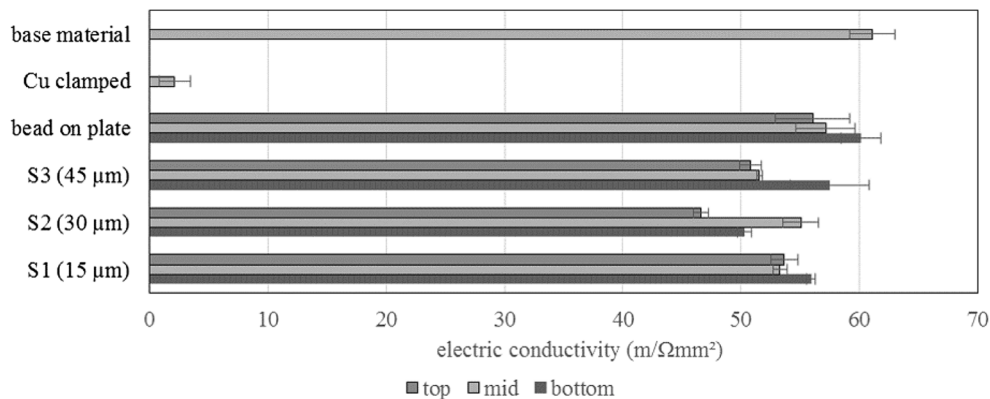


Fig. 11 Electric conductivity in $m/\Omega mm^2$ of different interlayer thicknesses, bead-on-plate (blind welding), clamped condition and base material. The value of the specific electric conductivity of Cu-DHP base material depends on the phosphorous content and is ranged between 55 and 45 $m/\Omega mm^2$ according to [8]



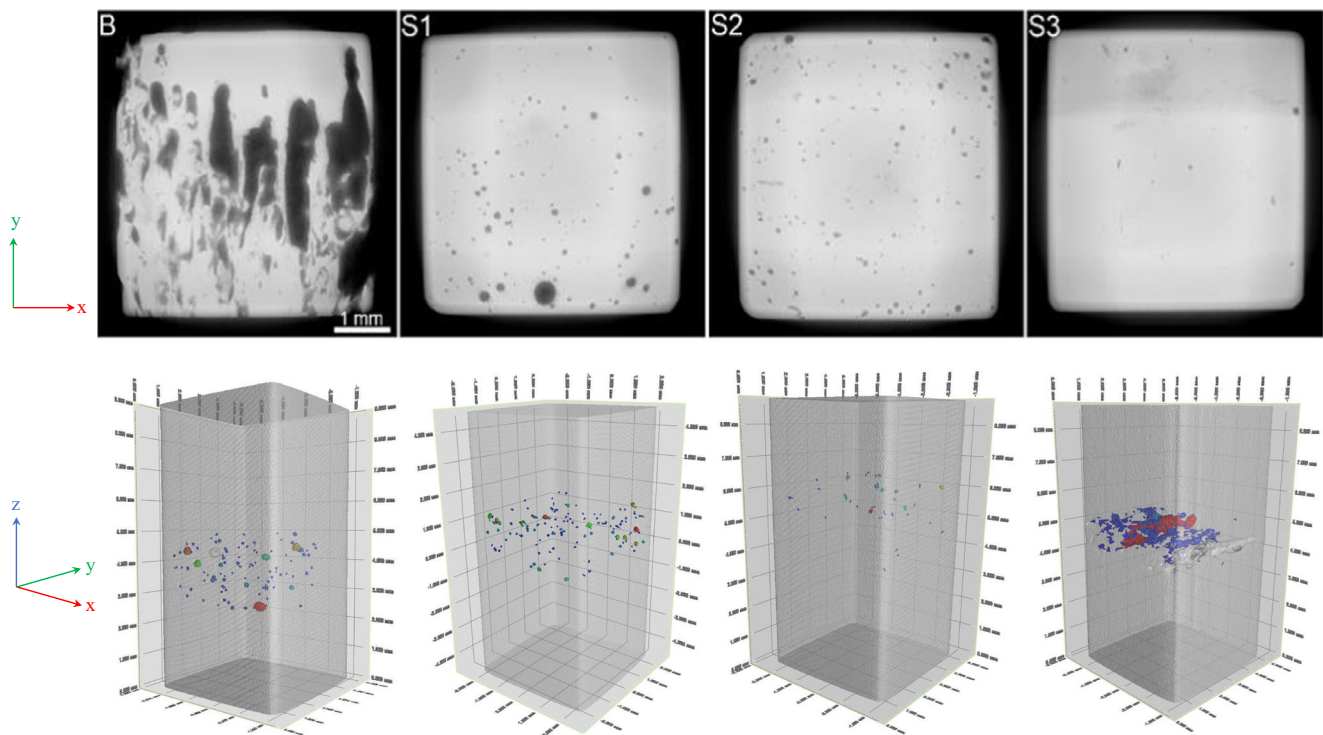


Fig. 12 CT investigation of the welded copper specimen at the bottom position (root position): **b** bead-on-plate; S1 interlayer thickness = 15 μm ; S2 interlayer thickness = 30 μm ; S3 interlayer thickness = 45 μm

EBW parameter variation (e.g. changing beam figure). However, defects could be reduced by introducing a filler material into the welding zone. APS was used to deposit filler materials. Consequently, EBW joints of thick-walled Cu-DHP alloys were successfully realised by adding thin APS Sn interlayers. Welding defects could be reduced significantly and a proper root formation could be maintained.

Using plasma interlayers led to some interesting findings:

- Local alloying (Sn) influences the viscosity, the surface tension and the melting interval. It can be assumed that these effects improve the root formation, due to an intended instable keyhole. By increasing the interlayer thickness, the melt viscosity decreases, which leads to an increased flow in root direction and more pronounced root formation.
- A Cu-Sn solid solution of the fusion zone could not be confirmed, due to partly evaporation of the Sn interlayer. The remaining Sn content could be observed in the root area of the cross-sections by LOM and was confirmed in EDX line scans.

Taking the decreasing viscosity with Sn contents from 0 to 10 wt% into account, it is assumed that the generated melting interval is the second positive driving effect of the viscopysical properties of the molten material and subsequent solidification.

- The partly liquid, partly solid fluid forms the root area and acts as a bead support for the more or less pure Cu melt in the majority of the fusion zone during solidification.
- The investigated interlayer thicknesses of 15, 30 and 45 μm are not influencing the mechanical and physical properties of the weld significantly. The increased porosity of the bead-on-plate welds, which is typical for spiking, led to a reduction of tensile strength. However, the tensile tests of the different Sn interlayer samples showed a resulting tensile strength of up to 90% of the base material.
- Contrary to assumptions, the specific electric conductivity has a minor dependency on the Sn interlayer thickness and porosity. The determined conductivity was lower than observed in bead-on-plate and base material, but showed a clear improvement compared to the state-of-the-art joints. A lower Sn alloying resulted in higher conductivities. CT measurements confirmed that local pore formation had no measurable influence on the specific electric conductivity.

To sum up, EBW brings a great benefit according to the electric conductivity of thick-walled copper components like electric conductive paths especially if it is compared to the state-of-the-art mechanical joint. Using APS to deposit a controlled Sn interlayer thickness is an easy and reliable method to improve EBW of thick-walled copper components.

In other words, EBW allows thinner copper parts, which are providing same amounts of electric current per cross sectional area. Using EBW has in particular a higher economic efficiency than the state-of-the art joining technique.

Acknowledgments Open access funding provided by Graz University of Technology. The research results of the comet K-project metal JOINing P1 were carried out in cooperation with Inocon Technologie GmbH, Eckert Effect Pigments, Air Liquide and Institute of Materials Science, Joining and Forming (IMAT) at Graz University of Technology.

The CT measurements were performed by Mr. Gusenbauer of the University of Applied Sciences Wels in Upper Austria.

Open Access This article is distributed under the terms of the Creative Commons Attribution 4.0 International License (<http://creativecommons.org/licenses/by/4.0/>), which permits unrestricted use, distribution, and reproduction in any medium, provided you give appropriate credit to the original author(s) and the source, provide a link to the Creative Commons license, and indicate if changes were made.

References

- Zhang LJ, Ning J, Zhang XJ, Zhang GF, Zhang JX (2015) Single pass hybrid laser-MIG welding of 4-mm thick copper without preheating. *Mater Des* 74:1–18. <https://doi.org/10.1016/j.matdes.2015.02.027>
- Kou S (2003) Solidification and liquation cracking issues in welding. *JOM* 55(6):37–42. <https://doi.org/10.1179/1362171815Y0000000031>
- Aalto H (1998) EB-welding of the copper canister for the nuclear waste disposal. Positiva report, pp 9–39
- Enzinger N, Loidolt P, Wiednig C, Stütz M, Sommitsch C (2017) Electron beam welding of thick-walled copper components. *Sci Technol Weld Join* 22(2):127–132. <https://doi.org/10.1080/13621718.2016.1204516>
- Pawlowski L (2008) Thermal spraying techniques. *The Science and Engineering of Thermal Spray Coatings*, pp 67–113. <https://doi.org/10.1002/9780470754085.ch3>
- Welding Institute of Canada, Drzeniek H, Lugscheider E (1986) *Advances in Thermal spraying*, pp 651–659. <https://doi.org/10.1016/B978-0-08-031878-3.50071-X>
- Sun Z, Karppi R (1996) The application of electron beam welding for the joining of dissimilar metals: an overview. *J Mater Process Technol* 59(3 SPEC. ISS):257–267. [https://doi.org/10.1016/0924-0136\(95\)02150-7](https://doi.org/10.1016/0924-0136(95)02150-7)
- Deutsches Kupferinstitut (2005) Cu-DH. <http://www.abmkupral.hu/letoltes/certec/Cu-DHP.pdf>. Accessed: 13-Mar-2017
- Amore S, Ricci E, Lanata T, Novakovic R (2008) Surface tension and wetting behaviour of molten Cu-Sn alloys. *J Alloys Compd* 452(1):161–166. <https://doi.org/10.1016/j.jallcom.2007.01.178>
- Tan M, Xiufang B, Xianying X, Yanning Z, Jing G, Baoan S (2007) Correlation between viscosity of molten Cu-Sn alloys and phase diagram. *Phys B Condens Matter* 387(1–2):1–5. <https://doi.org/10.1016/j.physb.2005.10.140>
- Bargel H-J, Schulze G (2005) *Werkstoffe*. Springer Verlag, Berlin
- Toma FL, Stahr C, Berger LM, Saaro S, Herrmann M, Deska D, Michael G (2010) Corrosion resistance of APS- and HVOF-sprayed coatings in the Al₂O₃-TiO₂ system. *J Therm Spray Technol* 19(1–2): 137–147. <https://doi.org/10.1007/s11666-009-9422-2>
- Song B, Dong S, Liao H, Coddet C (2015) Microstructure and wear resistance of FeAl/Al₂O₃ intermetallic composite coating prepared by atmospheric plasma spraying. *Surf Coat Technol* 268:24–29. <https://doi.org/10.1016/j.surfcoat.2014.06.055>
- Stummer M, Eichinger T, Stögmüller P, Enzinger N (2016) Improving the wetting behaviour of steel substrates by use of atmospheric pressure plasma. *Int J Mech Eng Autom* 3:482–490
- Hegemann D, Brunner H, Oehr C (2003) Plasma treatment of polymers for surface and adhesion improvement. *Nucl Instrum Methods Phys Res, Sect B* 208(1–4):281–286. [https://doi.org/10.1016/S0168-583X\(03\)00644-X](https://doi.org/10.1016/S0168-583X(03)00644-X)
- Tang S, Kwon O-J, Lu N, Choi H-S (2005) Surface characteristics of AISI 304L stainless steel after an atmospheric pressure plasma treatment. *Surf Coat Technol* 195:298–306. <https://doi.org/10.1016/j.surfcoat.2004.07.071>
- Eckart Effect Pigments (2017) Datasheet VP68036/G. Eckart Effect Pigments, Wesel
- Schultz H (1994) *Electron beam welding*, 1st edn. Woodhead Publishing, Sawston
- Xu M, Wang LV (2005) Universal back-projection algorithm for photoacoustic computed tomography. *Phys Rev E Stat Nonlinear Soft Matter Phys* 71(1). <https://doi.org/10.1103/PhysRevE.71.016706>
- Promet (2017) Stromschienen (Kupfer/Aluminium/Cuponal) - Produktpalette <http://www.promet.com/produkte/stromschienen.html>. Accessed: 13-Mar-2017
- Wei PS, Chuang KC, Ku JS, Debroy T (2012) Mechanisms of spiking and humping in keyhole welding. *IEEE Trans Compon Packag Manuf Technol* 2(3):383–394. <https://doi.org/10.1109/TCPM.2011.2178412>